PAPER

Check for updates

Environmental and industrial impacts of Cr(VI) in wastewater: high performance removal efficiency using novel ZIF-8 MOFs doped with cesium

Omnia I. Ali, [ID] *[a] Sheta M. Sheta, [ID] *[b] Eman A. Elmenofy,[a] A. T. Kandil[a] and Said M. El-Sheikh [ID] *[c]

Chromium is a heavy element that is extremely hazardous to both humans and the environment and is present in industrial waste. In this work, novel ZIF-8 MOFs doped with various molar ratios of cesium were prepared for the first time. Cs-2@ZIF-8 MOF was employed as an adsorbent material for removing Cr(VI) ions from wastewater. Several methods, like XRD, SEM/EDX, FT-IR, TEM, TGA, PL, BET, and XPS, were employed to characterize the physico-chemical and structural characteristics of the produced MOFs. The specific surface area of the ZIF-8 MOF was significantly enhanced from 1019.57 to 1204.95 $m^2\ g^{-1}$ when doped with Cs ions. SEM images revealed that the Cs-2@ZIF-8 MOF particles had a flower-like morphology. TEM images of the Cs-2@ZIF-8 MOF revealed a rhombic dodecahedron structure, with crystallite diameters between 20 to 30 nm. TGA investigation revealed that the thermal stability of the ZIF-8 MOF increased significantly after doping with cesium. The impact of key experimental factors on the removal of Cr(VI) ions using Cs-2@ZIF-8 was studied in a batch mode. The Cs-2@ZIF-8 MOF had an adsorption capacity of 61.05 mg g^{-1} for Cr(VI) adsorption, and even after four cycles, it maintained its removal ability. The Cr(VI) adsorption process employing the Cs-2@ZIF-8 MOF was exothermic and spontaneous, and it was in good agreement with the Freundlich isotherm and pseudo-second-order kinetics. The high recovery rate of Cr(VI) from actual water samples highlighted the excellent efficiency of the Cs-2@ZIF-8 MOF in wastewater remediation.

Environmental significance

Water often contains chromium, one of the most dangerous heavy metal pollutants, especially in its hexavalent form (VI). It poses significant hazards to the environment and human health, even at low levels. Development of novel adsorbent materials for removing Cr(VI) ions from wastewater is a hot research topic.

Introduction

Globally, chromium pollution is recognized as a major concern for the environment. Chromium-containing wastewater is produced in significant quantities through industrial activities, including leather tanning, electroplating, and mineral mining.[1] Water often contains chromium, one of the most dangerous heavy metal pollutants, especially in its hexavalent form (VI). It poses significant hazards to the environment and human health, even at low levels.[2,3] Cr(VI) is a highly carcinogenic and mutagenic agent that is detrimental to ecosystems because it is highly migratory and readily soluble in water.[4] Its toxic effects on humans include skin inflammation, lung cancer, and renal, liver, and stomach damage. Environmentally, Cr(VI) negatively impacts plant growth, reduces algal populations, and disrupts the ecological balance.[5] The Environmental Protection Agency's (EPA) maximum Cr(VI) limit in water is 0.1 mg L^{-1}.[6] Conventional techniques like ion exchange, chemical precipitation, and electrochemical separation are employed to extract heavy metals from aqueous solutions,[7–9] but these strategies face limitations such as low selectivity, slow kinetics, excessive costs, and secondary pollution. However, adsorption is an exciting alternative method that shows great promise because of its simplicity, affordability, and excellent removal efficiency, in particular for trace-level contaminants.[1,10,11] Heavy metals can be removed from water-based systems employing numerous adsorbents, such as activated carbon, metal–organic frameworks (MOFs), silica, zeolites, clays, and biopolymers.[12–14]

Over the past decades, MOFs have been recognized as substantially effective adsorbent materials for the remediation

[a]Department of Chemistry, Faculty of Science, Helwan University, Cairo, 11795, Egypt. E-mail: omniaibrahim95@gmail.com

[b]Department of Inorganic Chemistry, National Research Centre, Cairo, 12622, Egypt. E-mail: dr.sheta.nrc@gmail.com; Fax: +2-02-33370931; Tel: +20 1009697356

[c]Department of Nanomaterials and Nanotechnology, Central Metallurgical R & D Institute, Cairo, 11421, Egypt. E-mail: selsheikh2001@gmail.com; Tel: +20 1022316076

of heavy metals from aqueous solutions. Self-assembly techniques are used to create these structures, in which organic ligands act as linkers to join metal ions. MOFs offer significant advantages, including high porosities, geometries that facilitate high-yield production, low costs, versatile synthetic processes, and uniform pore-size distributions.[15–19] These unique properties have facilitated their application across various research fields, including adsorption, heterogeneous catalysis, drug delivery, photocatalysis, sensing, biosensing, and gas separation and purification.[20–24]

Zeolitic imidazolate frameworks (ZIFs) have gained attention for their exceptional capacity to remove heavy metals from wastewater. Their zeolite-like characteristics, such as superior porosity, exceptional resistance to chemical or heat changes, adjustable pore size, and high specific surface area, make them particularly effective.[11,25,26] Furthermore, ZIFs exhibit excellent thermal/chemical and water stabilities and are promising materials for removing various contaminants, including organic pollutants and oil emulsions; in particular,[26–30] ZIF-8 effectively adsorbs and reduces heavy metal ions in higher oxidation states. ZIFs play crucial roles in water treatment due to their high surface area, tunable porosity, and chemical stability in aqueous environments. Nevertheless, the adsorption performance of numerous ZIFs, including ZIF-8, requires additional improvements due to a lack of sufficient active sites. Incorporating other metal ions or guest molecules within MOFs to enhance the number of active sites and design new ZIF-8 MOFs possessing superior chemical and physical properties is a potential strategy for accomplishing this goal, thereby making them suitable for adsorption and water purification.[31–33] For instance, Sun *et al.* synthesized a copper-doped ZIF-8 MOF that demonstrated excellent adsorption performance towards tetracycline, which was 2.4 times better than that of the original ZIF-8.[34] Additionally, when ZIF-8 was doped with Co and Ni by Shen *et al.*,[35] the prepared doped MOFs had surface areas larger than that of pure ZIF-8 and their adsorption capacities to remove Cr(VI) were improved.[36]

In this study, the ZIF-8 MOF was doped for the first time with cesium ions at different molar ratios (Cs-1@ZIF-8 and Cs-2@ZIF-8 MOFs) to enhance its effectiveness in removing Cr(VI) from wastewater. Various characterization techniques, such as FT-IR, SEM/EDX, TEM, PL, XRD, BET, TGA, and XPS, were performed to evaluate the surface and structural characteristics of the prepared MOFs. In addition, the impact of key experimental factors on Cr(VI) adsorption employing the Cs-2@ZIF-8 MOF was studied along with its adsorption kinetics, isotherms, thermodynamics, and reusability.

Results and discussion

Characterization

XRD. Fig. 1a and b shows the X-ray diffraction patterns of ZIF-8 MOFs (pristine and doped). According to ZIF-8 MOF's XRD spectrum, ZIF-8 exhibited a theoretical XRD pattern that was consistent with the crystallographic MOF file (CCDC-602042).[37] The pristine ZIF-8 MOF's diffraction peaks were visible at 7.39°, 7.84°, 9.01°, 10.44°, 11.04°, 11.64°, 12.79°, 13.04°, 13.55°,

13.79°, 14.73°, 15.19°, 15.64°, 16.73°, 17.09°, 17.28°, 18.08°, 18.63°, 21.82°, 23.47°, 27.83°, and 29.07°. The obtained results were consistent with previous reports.[35,37–39] The XRD patterns of the Cs-doped ZIF-8 MOFs are displayed in Fig. 1a, which have the same signals of the ZIF-8 MOF.[28] Furthermore, adding Cs ions to the reaction mixture during the ZIF-8 crystal formation process had no impact on the framework structure of ZIF-8 materials. According to Table S1, the characteristic peaks of the original ZIF-8 MOF were not destroyed following cesium doping; nevertheless, their intensity was reduced, and they showed slight shifts to lower angles.[38] The observed shift in the Cs-2@ZIF-8 MOF sample somewhat increased as the molar ratio of cesium increased (Table S1). The stability of the Cs-2@ZIF-8 MOF after adsorption was examined *via* XRD analysis. The XRD pattern of the Cs-2@ZIF-8 MOF after Cr(VI) loading is shown in Fig. 1b, revealing two new peaks at 18.93° and 25.33° that were assigned to the typical CrO₃ peaks (JCPDS no. 72-0634),[40] confirming the Cr(VI) adsorption.[41] Furthermore, the XRD pattern for the Cs-2@ZIF-8 MOF following Cr(VI) adsorption revealed that the main peak of the Cs-2@ZIF-8 MOF was located at 10.99° and two new peaks appeared at 14.34° and 18.93°. Moreover, the intensity of the diffraction peaks was slightly reduced, and they were shifted to lower 2-theta angles (Table S1). In addition, the peaks at 12.94°, 13.49°, 13.69°, 17.04°, and 17.19° became broader after Cr(VI) adsorption on the Cs-2@ZIF-8 MOF. These findings demonstrated that the Cr(VI) adsorption procedure was accompanied by a minor decrease in the crystallinity of the Cs-2@ZIF-8 MOF.

FT-IR. As shown in Fig. 1c, FT-IR analysis was used to observe the functional groups and adsorptive processes of the ZIF-8 and Cs-doped ZIF-8 MOF samples. The peak at 1583 cm⁻¹ originated from the C=N stretching vibration of imidazole, whereas the peak at 1456 cm⁻¹ originated from the bending vibration of the methyl group.[11] The C–H bending mode could be the cause of the peak at 758 cm⁻¹, while C–N stretching was correlated with the peaks displayed at 1146 and 994 cm⁻¹. Furthermore, the peaks in the range of 1421–1310 cm⁻¹ were attributed to the whole ring stretching, while the out-of-plane bending vibrations of the imidazolate ring produced the peak at 693 cm⁻¹. The Zn–N bond vibration stretching that emerged at 420 cm⁻¹ indicated the successful synthesis of ZIF-8 MOFs, which included zinc atoms connected to the N-atoms of 2-methylimidazole.[28] A few peaks in the FT-IR spectra of the Cs-2@ZIF-8 MOF (Fig. 1c) showed minor changes (Table S2). Furthermore, two additional peaks at 828 and 738 cm⁻¹ were observed following the doping of the ZIF-8 MOF with Cs ions. Also, the peaks at 1669 and 672 cm⁻¹ showed a significant decrease in their strength.

SEM-EDX. Investigation and evaluation of the morphological characteristics of the cesium-doped ZIF-8 MOF samples were performed using FESEM analysis. SEM images, as shown in Fig. 2a and b obviously demonstrate that Cs-1@ZIF-8 and Cs-2@ZIF-8 MOFs exhibited a petal-like (flower-like) shape with a smooth surface, in which the MOFs were shaped as a rhombic dodecahedron due to the agglomeration of the MOFs.[35] These findings demonstrate that the ZIF-8 MOF's surface shape and framework structure remained unchanged when the doping ratio of Cs ions was increased.
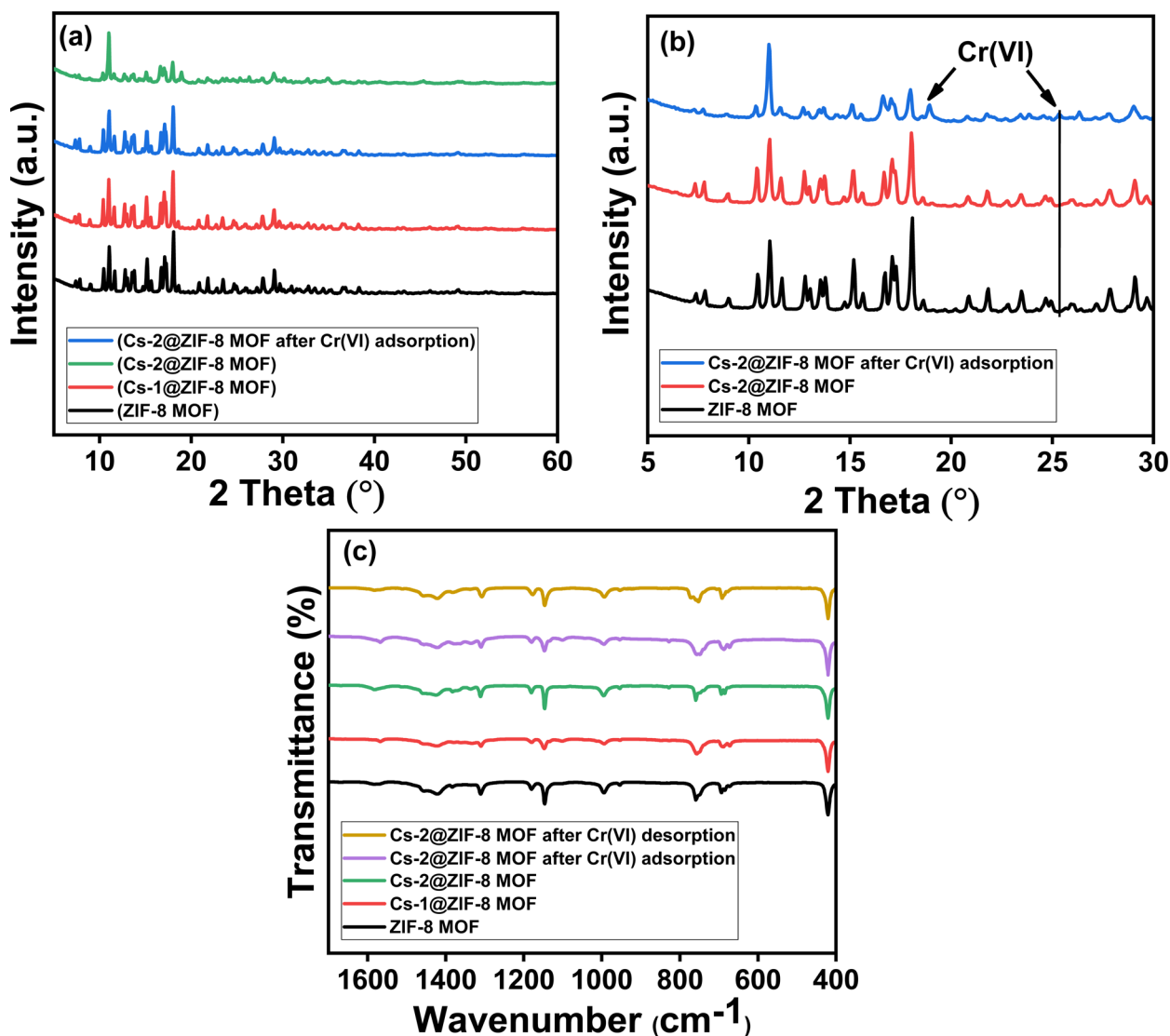
Fig. 1 (a) XRD patterns of ZIF-8, Cs-1@ZIF-8, and Cs-2@ZIF-8 before and after Cr(vi) adsorption (5° to 60°). (b) XRD patterns of ZIF-8 and Cs-2@ZIF-8 (before and after Cr(vi) adsorption) (5° to 30°). (c) FT-IR spectra of ZIF-8, Cs-1@ZIF-8, and Cs-2@ZIF-8 before and after Cr(vi) adsorption and desorption.

Fig. S1a displays the EDX spectrum, revealing the composition of the elements in the Cs-2@ZIF-8 sample. According to the EDX data, the primary chemical elements—C, N, Zn, and Cs—were present. The EDX elemental mapping of the Cs-2@ZIF-8 sample in Fig. S1a shows yellow spots corresponding to the Cs element, suggesting its presence throughout the ZIF-8 MOF structure. It was thus verified by the EDX mapping analysis that Cs ions were successfully doped into the ZIF-8 MOF.

SEM and EDX analyses were employed to examine the changes in the surface morphology and elemental composition of the Cs-2@ZIF-8 MOF following the Cr(vi) adsorption. As illustrated in Fig. 2c, the Cs-2@ZIF-8 MOF framework exhibited no apparent collapse or decomposition, but the particles showed a slight agglomeration. At the same time, the EDX spectrum and elemental mapping analysis of the Cs-2@ZIF-8 MOF following chromium adsorption (Fig. S1b) confirmed that the surface of the Cs-2@ZIF-8 MOF contained Cr(vi).

TEM. Fig. 2d and e displays the TEM images of the Cs-2@ZIF-8 MOF, which show that the sample had irregular tetragonal and hexagonal structures. TEM images also indicated that the surface of the Cs-2@ZIF-8 MOF was agglomerated and rough. The images revealed that the diameter of the Cs-2@ZIF-8 MOF crystallite was between 20-30 nm. The analysis of the particle size distribution of the Cs-2@ZIF-8 MOF is illustrated in Fig. 2f.

XPS. The electronic structure and chemical oxidation states of the Cs-2@ZIF-8 adsorbent surface (Fig. 3a) were investigated using X-ray photoelectron spectroscopy,[42,43] which revealed the presence of the elements Zn, C, N and O. The Zn 2p spectra revealed two peaks at 1021.77 and 1044.74 eV for $2p_{3/2}$ and $2p_{1/2}$, respectively (Fig. 3b), which agreed with a prior finding by Shen *et al.*[35] It was determined that the prominent characteristic peak in Fig. 3c, with a binding energy of 284.85 eV, originated from the imidazole side chain's C–C
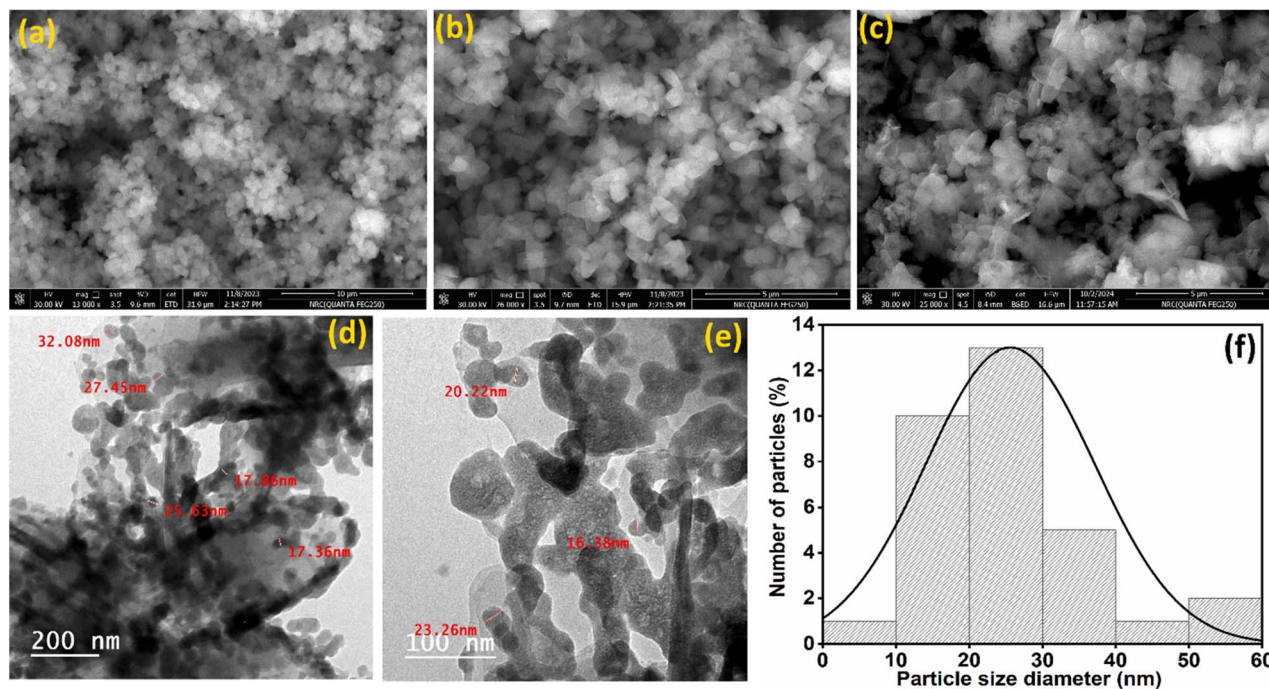
Fig. 2 (a)–(c) SEM images of (a) Cs-1@ZIF-8, (b) Cs-2@ZIF-8, and (c) Cs-2@ZIF-8 after Cr(VI) adsorption, (d) and (e) TEM images of Cs-2@ZIF-8, and (f) particle-size distribution of Cs-2@ZIF-8.
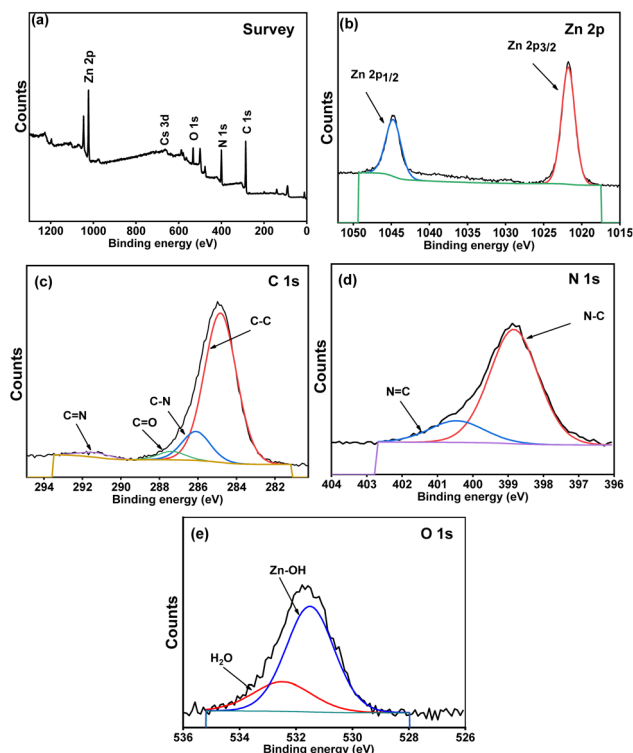

Fig. 3 XPS spectra of the Cs-2@ZIF-8 MOF: (a) survey, (b) Zn 2p, (c) C 1s, (d) N 1s, and (e) O 1s.

bond. The C–N, C=O, and C=N bonds are responsible for the three peaks at 285.92, 287.38, and 291.39 eV, respectively.[34,44,45] The peaks of the imidazole ring (C=N and C–N), located at

400.45 and 398.84 eV, respectively, were isolated from fitting of the N 1s spectra (Fig. 3d).[46] The O 1s spectra of the Cs-2@ZIF-8 MOF produced signals corresponding to H_2O and Zn–OH at 532.5 and 531.5 eV, respectively.[47] As seen in Fig. 3a, the absence of a distinct peak for Cs ions in the sample survey suggests that only a tiny quantity of Cs ions may have contributed to the synthesis of the doped MOF.

TGA. The thermal stability of ZIF-8 and Cs-2@ZIF-8 MOFs was investigated using TGA/dTA in a nitrogen environment between 35 °C and 790 °C (Fig. 4a). Three major phases of weight loss were identified throughout the calcination process by the TGA analysis of the ZIF-8 MOF. The initial mass loss occurred at 258 °C and was attributed to the sample's surface water desorption; at this point, the weight loss was 10%. The second weight loss, which was 15% and happened at 398 °C due to release of absorbed unreacted molecules in the ZIF-8 structure's pores, such as 2-methylimidazole as organic linkers.[45] The third weight-loss stage occurred at 784 °C and was around 20% due to the decomposition of the skeletal structure of the ZIF-8 MOF broke down and disintegrated into ZnO as the temperature rose[38] and about 25% of the residual mass remained, which was connected to the MOF's metal content. Similarly, the TGA curve of the Cs-2@ZIF-8 MOF showed an initial weight loss at 258 °C, with a reduction in weight of around 10% because of the dissolution of water molecules. In the second stage, which lasted until 398 °C, there was a 15% decrease in weight due to the breakdown of 2-methylimidazole from the framework of the sample. In addition, in the third stage, the structure of the doped MOF was destroyed at high temperature into zinc oxide and cesium oxide. At this stage, the weight loss was 20% at 784 °
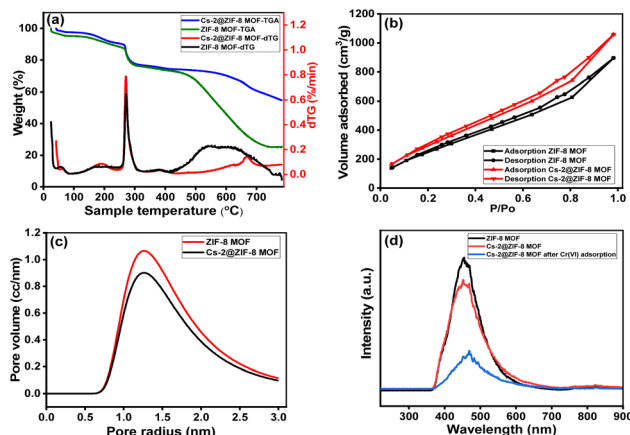
© 2025 The Author(s). Published by the Royal Society of Chemistry

Environ. Sci.: Adv., 2025, **4**, 1622–1632 | **1625**

Fig. 4 (a) TGA analysis, (b) BET analysis, and (c) pore sizes of ZIF-8 and Cs-2@ZIF-8 MOFs. (d) Photoluminescence spectra of the ZIF-8 MOF and Cs-2@ZIF-8 MOF (before and after Cr(VI) adsorption).

C. The residue was about 55%, which was connected to the Cs-2@ZIF-8 MOF's metal content.

BET. N_2 adsorption/desorption isotherm plots are shown in Fig. 4b, which were based on the porosity analysis of the produced ZIF-8 and Cs-2@ZIF-8 MOFs. Mesopores were most likely present in the samples because the produced ZIF-8 and Cs-2@ZIF-8 MOFs showed a type IV isotherm. According to the BET analysis, the specific surface area of ZIF-8 increased from 1019.57 m^2 g^{-1} to 1204.95 m^2 g^{-1} after doping with cesium ions, indicating that Cs doping enhanced the porosity and surface accessibility of the material. The pore volumes of ZIF-8 and Cs-2@ZIF-8 MOFs were also determined, and they were 0.96 and 1.14 cm^3 g^{-1}, respectively. The produced ZIF-8 and Cs-2@ZIF-8 MOFs exhibited micro- and meso-porous structures with pore size ranging from 0.75 to 3.0 nm, and an average pore radius of 1.26 nm (Fig. 4c).

Photoluminescence analysis. The photoluminescence (PL) spectra of the ZIF-8 MOF, Cs-2@ZIF-8 MOF, and Cs-2@ZIF-8 MOF following Cr(VI) adsorption, were obtained using a 320 nm excitation wavelength (Fig. 4d). To evaluate the ability of MOFs to distinguish photoinduced electron–hole pairs, PL analysis was performed. It is commonly known that the electron–hole recombination rate is measured by the PL intensity. According to Malik *et al.*,[48] a high intensity of PL translates into a greater rate of recombination, which shortens the time needed for electron–hole separation. The highest intensities of the ZIF-8 MOF, Cs-2@ZIF-8 MOF, and Cs-2@ZIF-8 MOF emission spectra after Cr(VI) adsorption were roughly 455, 452, and 470 nm, respectively. Fig. 4d shows that the ZIF-8 MOF had the PL maximum intensity, suggesting its highest electron–hole recombination rate. However, after cesium doping, the significant reduction in the peak intensity of the Cs-2@ZIF-8 MOF suggested that the electron–hole separation time was longer. Furthermore, the Cs-2@ZIF-8 MOF after Cr(VI) adsorption showed the lowest PL intensity.

Adsorption studies

Comparison between the prepared adsorbents. The removal efficiencies of ZIF-8, Cs-1@ZIF-8, and Cs-2@ZIF-8 MOFs for
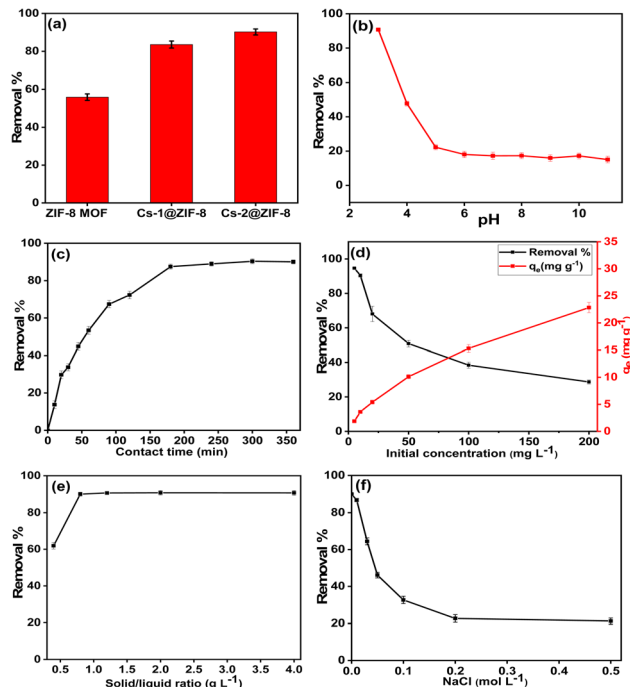

Fig. 5 (a) Comparison of removal% for the prepared adsorbents; the impact of various parameters on Cr(VI) removal using the Cs-2@ZIF-8 MOF, (b) initial pH, (c) contact time, (d) initial chromium concentration, (e) solid/liquid ratio, and (f) ionic strength.

Cr(VI) ions were compared (Fig. 5a) under identical conditions of 0.02 g of sample, an initial metal concentration of 10 mg L^{-1}, contact time of 4 h, pH 3, and at 25 °C. The adsorption efficiencies achieved for Cr(VI) using ZIF-8, Cs-1@ZIF-8, and Cs-2@ZIF-8 MOFs were 55.92%, 83.57%, and 90.23%, respectively. Notably, the Cs-2@ZIF-8 MOF achieved the maximum removal efficiency because the Cs-2@ZIF-8 MOF had a larger surface area, as revealed from the BET results, and a greater number of active sites resulting from cesium ion doping.[35] Therefore, for the following studies, the Cs-2@ZIF-8 MOF was chosen as the best adsorbent.

Effect of initial pH. A crucial variable that affects the absorption efficacy is the solution's initial pH, and it can strongly influence the solubility of metal ions as well.[49] The rate of Cr(VI) ion adsorption and elimination under various pH ranges was investigated (Fig. 5b). Additionally, Cs-2@ZIF-8 MOF's point of zero charge (pH_{pzc}) was evaluated and found to be 8.3 (Fig. S2). According to the pH_{pzc} value, at pH <8.3, the Cs-2@ZIF-8 MOF's surface charge was positive. Consequently, in these conditions, the Cs-2@ZIF-8 MOF exhibited a significant electrostatic attraction with Cr(VI) ions. The highest Cr(VI) ion adsorption was observed at pH 3.0, as shown in Fig. 5b, and the removal percentage diminished at a higher pH. Beginning at pH 6, the removal rate demonstrated a slight decrease as the pH increased. In this regard, various forms of chromium like H_2CrO_4 (chromic acid), $HCrO_4^-$ (hydrogen chromate ions), and CrO_4^{2-} (chromate ions) at various pH levels were evaluated. The quantity of H^+ in the water was higher at a pH of 3, which induced protonation reactions on the adsorbent surface and the

adsorption of chromium ions *via* electrostatic attraction. This process can enhance the adsorption and removal of Cr(vi) ions. However, as the pH continued to rise, additional OH$^-$ was produced, which competed for adsorption with CrO$_4^{2-}$ and other anions, leading to a decline in the rate of Cr(vi) adsorption and removal. Because there was a higher H$^+$ content in the water at pH = 3, protonation reaction occurred on the adsorbent surface, and chromium ions were drawn to it by electrostatic attraction. This may help the Cr(vi) ions get adsorbed and removed. The adsorption and Cr(vi) removal rate decreased steadily as the pH increased because more OH$^-$ was produced, which competed for adsorption with CrO$_4^{2-}$ and other anions.[4,13] These results revealed that different mechanisms are responsible for the removal of Cr(vi) ions using the Cs-2@ZIF-8 MOF.

Effect of contact time. Fig. 5c illustrates how the contact time impacts the Cr(vi) adsorption using the Cs-2@ZIF-8 MOF for a starting Cr(vi) concentration of 10 mg L^{-1}. At various time points (10, 15, 30, 45, 60, 90, 120, 180, 240, 300, and 360 min), the Cr(vi) ion removal using Cs-2@ZIF-8 was investigated. The uptake equilibrium of Cr(vi) ions was established after 300 min, and no remarkable changes were observed for higher reaction times. In the studies that followed, 300 min was selected as the reaction time needed to achieve equilibrium adsorption.

Effect of initial concentration. Fig. 5d displays the removal percentage of Cr(vi) ions using the Cs-2@ZIF-8 MOF according to the initial chromium ion concentration. At pH 3, the Cs-2@ZIF-8 MOF and Cr(vi) ions with varying starting Cr(vi) concentrations (5–200 mg L^{-1}) were in contact for 300 min. Fig. 5d demonstrates that when the starting Cr(vi) concentration increased, the Cr(vi) removal percentage declined. As an adsorbent with a specified quantity of sites that are active, the Cs-2@ZIF-8 MOF caused a decrease in the adsorption because the active sites became saturated at larger concentrations of Cr(vi) ions. However, Fig. 5d establishes that the capacity of the Cs-2@ZIF-8 MOF to adsorb Cr(vi) ions increased as the starting concentration of these ions was increased. The interpretation of this behavior is the rising gradient in Cr(vi) ion concentration, which surpasses the barrier of mass transfer of the ions of Cr(vi) that occurs between ions of Cr(vi) and Cs-2@ZIF-8 MOF.[50,51]

Effect of solid/liquid ratio. One critical component that significantly affects the removal efficiency is the solid/liquid ratio. Fig. 5e displays the solid/liquid ratio effect of the Cs-2@ZIF-8 MOF (0.4, 0.8, 1.2, 2, and 4 g L^{-1}) on the removal of Cr(vi) ions. The findings demonstrated that increasing the solid/liquid ratio in the range of 0.4 to 4.0 g L^{-1} improved the removal of Cr(vi) ions. The enhanced removal effectiveness of Cr(vi) may be due to the rise in active sites on the Cs-2@ZIF-8 MOF surface for Cr(vi) adsorption. At solid/liquid ratios larger than 0.8 g L^{-1}, no observable change in the removal efficiency of Cr(vi) was produced, suggesting that the process of adsorption had reached its maximal capacity under the specified conditions. The surface area of the Cs-2@ZIF-8 MOF did not increase as a result of the aggregation of the adsorbent particles.[52]

Effect of ionic strength. The effect of ionic strength on Cr(vi) removal by the Cs-2@ZIF-8 MOF is depicted in Fig. 5f. As demonstrated, the removal percentage dropped as the ionic strength increased from 0.01 to 0.5 mol L^{-1}. Because the ionic strength reduced the probability of Cr(vi) ions getting into interaction with the adsorbent, increasing the concentration of NaCl probably resulted in a lower removal percentage of Cr(vi) ions. Additionally, the amount of Cr(vi) ions adsorbed at the active sites on the Cs-2@ZIF-8 MOF surface decreased because the Cr(vi) ions were in competition for adsorption with the coexisting anions.[4]

Interference studies. This study assessed the impact of different coexisting cations and anions on the removal of Cr(vi) (5 mg L^{-1}) using the Cs-2@ZIF-8 MOF (Table 1). Using 0.02 g of the Cs-2@ZIF-8 MOF at pH 3.0, the impact of a few common ions coexisting with Cr(vi) was examined. The number of interference ions that caused a change in the Cr(vi) removal percentage to be less than 95% was considered the tolerance limit. Natural water contamination often involves a complex mixture of geochemical ions, both positively (cations) and negatively (anions) charged. These ions can significantly influence the adsorption process of heavy metals like chromium. Therefore, assessing the impact of these coexisting ions on the performance of the Cs-2@ZIF-8 MOF in removing heavy metals from water was crucial for determining its practical applicability in water treatment.[53] Results demonstrated that anions interfered more than cations when removing Cr(vi) using the Cs-2@ZIF-8 MOF. The reduction in the removal percentage could be ascribed to the anions possessing a charge analogous to that of the chromium species, leading to a competition for the active sites on the surface of the adsorbent. Consequently, the availability of sites that are active for Cr(vi) ions was diminished.

Sorption isotherms

The linear plots of the four isotherm models that were tested for Cr(vi) adsorption on the Cs-2@ZIF-8 MOF are demonstrated in Fig. S3. Table 2 provides the parameter values for each model, among which the correlation coefficient (R^2) values of the isotherm model for Freundlich adsorption was the maximum at 0.9984. These results indicated that the Cs-2@ZIF-8 MOF conforms to the Freundlich adsorption model during the Cr(vi) adsorption, demonstrating the surface heterogeneity of the Cs-2@ZIF-8 MOF and its multilayer Cr(vi) adsorption. Furthermore, the prepared Cs-2@ZIF-8 MOF showed favorable

Table 1 Effect of foreign ions on Cr(vi) removal using the Cs-2@ZIF-8 MOF

Foreign ions	Ratio of Cr(vi) to foreign ions	Removal%
Cl$^-$	1 : 700	95.55
NO$_3^-$	1 : 500	95.89
CO$_3^{2-}$	1 : 100	95.10
HCO$_3^-$	1 : 300	95.67
SO$_4^{2-}$	1 : 650	95.92
K$^+$	1 : 800	95.97
Na$^+$	1 : 400	95.23
Ca^{2+}	1 : 200	95.66
Mg^{2+}	1 : 200	95.75

© 2025 The Author(s). Published by the Royal Society of Chemistry

Environ. Sci.: Adv., 2025, **4**, 1622–1632 | **1627**

Table 2 Calculated parameters for the Freundlich, Langmuir, D–R, and Temkin isotherm models for the adsorption of Cr(vi) onto the Cs-2@ZIF-8 MOF

Isotherm model	Parameters	Temperature			
		25 °C	35 °C	45 °C	55 °C
Freundlich	K_F	9.82	8.11	7.14	5.45
	$1/n$	0.38	0.39	0.36	0.37
	R^2	0.9984	0.9986	0.9987	0.9937
Langmuir	K_L (L mg^{-1})	0.38	0.33	0.38	0.32
	q_{max} (mg g^{-1})	61.05	45.85	33.59	29.11
	R^2	0.9068	0.9503	0.9364	0.9141
	R_L	0.105	0.088	0.079	0.075
D–R	K_{D-R}	41.38	35.69	25.89	20.07
	β	0.13	0.18	0.19	0.22
	E (kJ mol^{-1})	1.96	1.67	1.62	1.51
	R^2	0.9473	0.9585	0.9573	0.8909
Temkin	K_T (L mg^{-1})	1.55	1.71	1.70	1.69
	b_T (J mol^{-1})	400.80	434.45	571.11	782.65
	R^2	0.8892	0.9253	0.9517	0.8765

adsorption for Cr(vi) since the n values were greater than one (Table 2). As observed, the Freundlich constant, K_F, declined with the increase in temperature, demonstrating that the adsorption process was exothermic.[54] Applying the Langmuir model, the Cs-2@ZIF-8 MOF at 25 °C showed a maximum Cr(vi) adsorption capacity of 61.05 mg g^{-1}. Table 3 further compares the q_{max} values of the Cs-2@ZIF-8 MOF for removing Cr(vi) with those obtained from earlier investigations. It is clear from the data that the Cs-2@ZIF-8 MOF shows great promise as an adsorbent compared with other adsorbents. Since the values of $R_L < 1$, the results in Table 2 suggest that the Cr(vi) adsorption process utilizing the Cs-2@ZIF-8 MOF was favorable. Also, the physisorption nature of the adsorption of Cr(vi) using the Cs-2@ZIF-8 MOF was demonstrated since the determined E values using the D–R model were smaller than 8 kJ mol^{-1}. Additionally, the values of Temkin isotherm K_T and b_T constants are summarized in Table 2. As shown, the obtained low b_T values indicate a weaker electrostatic interaction between the Cs-2@ZIF-8 MOF surface and Cr(vi) ions.

Table 3 Comparison of q_{max} of Cr(vi) reported in the current work with other reported works

Adsorbents	q_{max} (mg g^{-1})	References
Cu(i)-MOF	95.92	1
Zn-Co-SLUG-35 MOF	68.5	55
SLUG-21 MOF	37	56
1-ClO$_4$ MOF	62.9	57
1-NO$_3$ MOF	60	58
MIL101(Fe)-Na$_2$CO$_3$	20	4
ZIF-67	13.34	59
ZIF-8 MOF	0.15	36
ZIF-8-EGCG	22.46	60
ZIF-8/NH$_2$/Mg(OH)$_2$/GO	4.88	13
Fe$_3$O$_4$/biochar/ZIF-8	125	61
ZIF-8@ZIF-8/PAN nanofibers	39.68	30
Cs-2@ZIF-8 MOF	61.05	This work

Sorption kinetics

By estimating and fitting the findings of the kinetic models in the adsorption investigations (intraparticle diffusion, pseudo-first-order, pseudo-second-order, and Elovich), it was possible to determine the controlling mechanism of the adsorption process. The kinetic parameters for the adsorption of Cr(vi) utilizing the Cs-2@ZIF-8 MOF are presented in Table 4, while Fig. 6a and S4 show the results obtained. Also, by comparing the R^2 values, it is clear that, in comparison to other models, the pseudo-second-order model offered the best fit for Cr(vi) adsorption utilizing the Cs-2@ZIF-8 MOF. Furthermore, the calculated values ($q_{e,cal}$) and the experimental values ($q_{e,exp}$) for the Cr(vi) equilibrium capacity using the pseudo-second-order kinetic model were remarkably close. The intraparticle

Table 4 Calculated parameters for the pseudo-1st order, pseudo-2nd order, intraparticle diffusion, and Elovich models for Cr(vi) adsorption onto the Cs-2@ZIF-8 MOF

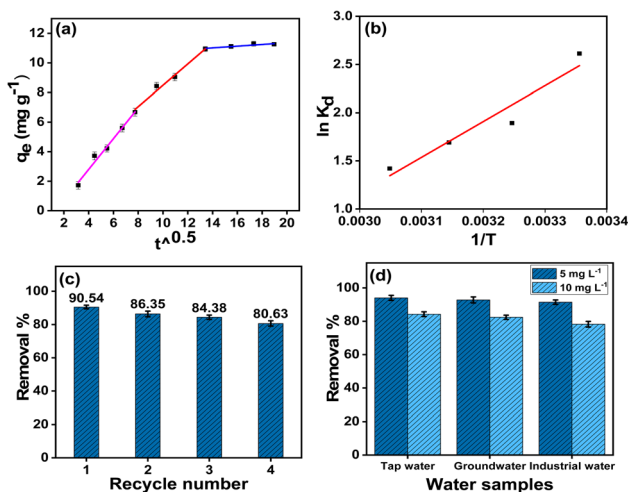| Kinetics models	Parameters	Values
Pseudo-1st order	k_1 (min^{-1})	0.02
	$q_{e(exp)}$ (mg g^{-1})	11.35
	q_e (mg g^{-1})	9.91
	R^2	0.9907
Pseudo-2nd order	k_2 (g mg^{-1} min^{-1})	0.001
	q_e (mg g^{-1})	13.61
	R^2	0.9967
Intraparticle diffusion		
1st step	K_i (mg g^{-1} min$^{-1/2}$)	1.04
	C	1.37
	R^2	0.9835
2nd step	K_i (mg g^{-1} min$^{-1/2}$)	0.72
	C	1.28
	R^2	0.9886
Elovich	α (mg g^{-1} min^{-1})	0.39
	β (mg g^{-1})	0.32
	R^2	0.9602

Fig. 6 (a) Intraparticle kinetic model, (b) thermodynamics plot. (c) Reusability, and (d) recovery of Cr(VI) from real water samples using the Cs-2@ZIF-8 MOF.

diffusion model sheds light on the mechanism of diffusion. The adsorption rate is solely determined by intraparticle diffusion when the intraparticle diffusion plot crosses the origin.[62] However, the two linear zones shown in Fig. 6a established that a multi-step mechanism governed the Cr(VI) adsorption. Cr(VI) initially diffused rapidly on the exterior surface of the Cs-2@ZIF-8 MOF, then underwent intraparticle diffusion. The second activity involved the migration of Cr(VI) ions from the outer surface of the Cs-2@ZIF-8 MOF into the pores, where the actual adsorption process proceeded. Additionally, the Elovich constant values α and β are displayed in Table 4. It could be seen from the α and β values that the degree of adsorption diminished over time due to the saturation of the Cs-2@ZIF-8 MOF surface with Cr(VI) ions.[63]

Thermodynamic studies

Four temperatures (298, 308, 318, and 328 K) were used in the adsorption studies to explore the thermodynamics of Cr(VI) adsorption utilizing the Cs-2@ZIF-8 MOF. The estimated parameters are displayed in Fig. 6b. Table 5 indicates that the Cr(VI) adsorption occurred spontaneously within the temperature range under investigation, as shown by the negative values of ΔG°. Also, an exothermic character of the adsorption of Cr(VI) onto the Cs-2@ZIF-8 MOF was suggested by the ΔH° value being negative, implying that Cr(VI) adsorption was favorable at lower temperatures. The rise in temperature weakened the interaction between ions of Cr(VI) and Cs-2@ZIF-8 MOF molecules, and this agreed with the results of temperature effects. In addition, an

increased order at the Cs-2@ZIF-8 MOF/solution interface during the adsorption of Cr(VI) was shown by the negative value of ΔS°.[1]

Recovery and reusability

For industrial operations, recovery and reusability of the Cs-2@ZIF-8 MOF are crucial. For three hours, 0.02 g of Cr(VI)-loaded The Cs-2@ZIF-8 MOF was shaken with 10 mL of various desorption solutions, including solutions of 0.01 mol L^{-1} NaOH, NaHCO$_3$, BaCl$_2$, and Na$_2$CO$_3$, in order to examine the desorption process. Following the determination of the desorbed quantities of Cr(VI), eqn (1) was used to compute the desorption efficiencies. It was found that NaHCO$_3$ was the most effective solution that could be used for the quantitative desorption of Cr(VI) ions from the Cs-2@ZIF-8 MOF. To test the produced Cs-2@ZIF-8 MOF's potential for reusability, adsorption/desorption cycles were performed. Fig. 6c makes it evident that the recycling procedure caused a minor drop in the adsorption efficiency. Nonetheless, the results showed that the Cs-2@ZIF-8 MOF had a respectable four-cycle reuse capability.

$$R_{des} = \frac{D_{des}}{A_{ads}} \times 100 \tag{1}$$

In addition, the XRD patterns of the Cs-2@ZIF-8 MOF post-desorption and reuse were examined to evaluate its structural stability, as illustrated in Fig. S5. Minimal variations were noted in the XRD patterns, suggesting that the Cs-2@ZIF-8 MOF preserved its crystalline structure and was stable after multiple adsorption–desorption cycles.

Application to real samples

The Cs-2@ZIF-8 MOF was used to extract Cr(VI) from actual water samples, including tap water, groundwater, and industrial water (Abu-Zaable Fertilizers and Chemicals Co.), in order to assess its analytical applicability. The recovery of Cr(VI) from the tested water samples was examined at pH 3 by adding standard Cr(VI) quantities (5 and 10 mg L^{-1}) to a 25 mL aliquot of the water sample. Fig. 6d displays the recovery findings for Cr(VI). The range of 78% to 94% for the Cr(VI) percentage recovery from water samples indicates that the adsorbent Cs-2@ZIF-8 MOF is appropriate for extracting Cr(VI) from real water samples.

Sorption mechanism

The XPS of the Cs-2@ZIF-8 MOF after Cr(VI) adsorption was further analyzed to explain the sorption mechanism of Cr(VI) on the Cs-2@ZIF-8 MOF. As shown in Fig. S6a, characteristic peaks corresponding to Zn, C, N, O, and a new peak for Cr 2p were observed, confirming the successful adsorption of Cr(VI) species onto the MOF surface. The C 1s spectrum after chromium adsorption (Fig. S6c) revealed variations in peak intensities at 284.8 eV, 285.79 eV, and 291.39 eV, attributed to C–C, C–N, and C=N bonds, respectively. Notably, the peak at 286.46 eV disappeared after adsorption, indicating chemical changes in the carbon environment. The N 1s spectrum is shown in Fig. S6d. It

Table 5 Thermodynamic parameters for Cr(VI) adsorption onto the Cs-2@ZIF-8 MOF

ΔH° (kJ mol^{-1})	ΔS° (J mol^{-1} K^{-1})	ΔG° (kJ mol^{-1})			
		298 K	308 K	318 K	328 K
−30.92	−83.08	−61.62	−53.31	−45.00	−36.69

can be seen that the peak areas of C–N and C=N decreased after Cr(VI) adsorption, along with the appearance of a new peak at 406.76 eV belonging to the protonated =N⁺ groups.[64] This suggests that protonated nitrogen sites (=N⁺) facilitated electrostatic interactions with the negatively charged Cr(VI) species. In the O 1s spectrum (Fig. S6e), the peaks around 533.34 and 531.96 eV were signals of adsorbed H_2O and Zn–OH, respectively.[65] As noted, the peak of H_2O was shifted, and the relative area ratio for the Zn–OH peak increased from 74.5% to 78.31% after Cr(VI) adsorption, indicating the involvement of OH groups in the adsorption process through chemical interaction.[30] The deconvolution of the Cr 2p spectrum is shown in Fig. S6f. The main peaks at 585.93, 577.16, 579.65, and 588.29 eV were assigned to Cr(III) $2p_{1/2}$, Cr(III) $2p_{3/2}$, Cr(VI) $2p_{3/2}$, and Cr(VI) $2p_{1/2}$, respectively,[65] which indicated the coexistence of Cr(VI) and Cr(III) species. These results indicated that during the adsorption process, Cr(VI) was adsorbed on the surface-active sites, such as Zn–OH through anion exchange and the protonated N through electrostatic attraction, and finally a fraction of Cr(VI) species was reduced to Cr(III) by the N groups of the Cs-2@ZIF-8 MOF.[64,65]

Furthermore, Fig. 1c shows the Cs-2@ZIF-8 MOF FT-IR spectrum following adsorption. It is evident that the spectrum has changed, with a slight decrease in the intensity of some MOF peaks and noticeable shifts in others (Table S2), confirming the elimination of chromium. The C=N stretching peak was shifted to 1568 cm⁻¹ following Cr(VI) adsorption, which could be because of the interaction with the hydrogen chromate ions,[11] suggesting complexation or electrostatic attraction during the adsorption process. The spectrum also revealed a new peak at 1100 cm⁻¹, which was assigned to the asymmetric stretching of the (CrO_3) group.[66] In addition, the peaks at 1668 and 1511 cm⁻¹ were vanished. Additionally, upon the adsorption of Cr(VI) on the Cs-2@ZIF-8 MOF, the peaks at 694 and 685 cm⁻¹ seemed to become a broad peak at 687 cm⁻¹. These findings validated that chromium was successfully adsorbed onto the Cs-2@ZIF-8 MOF.[5,67,68]

Also, as detailed in the "effect of initial pH" section, Cr(VI) adsorption using the Cs-2@ZIF-8 MOF proceeded *via* electrostatic attraction at low pH values. The optimal adsorption occurred at pH 3, where the increased concentration of H⁺ ions enhanced the electrostatic interaction between the protonated N functional groups of imidazolate ligands and negatively charged chromium species, primarily $HCrO_4^-$ species.[13,64] It is clear from previous results that both physical and chemical adsorption of Cr(VI) onto the Cs-2@ZIF-8 MOF occurred.

Experimental

Instruments

The description for all instruments is provided in the SI file Appendix A.

ZIF-8 and Cs-doped ZIF-8 MOF syntheses

The precipitation method was used to prepare ZIF-8 MOFs in accordance with a previous report.[35] In this study, the following steps were carried out: a solution of zinc nitrate in H_2O (0.5 mol L⁻¹, 10 mL) was gradually mixed with an aqueous solution of 2-methylimidazole (1.0 mol L⁻¹, 50 mL) in a molar ratio of 1 : 10 while being continuously stirred. The reaction was conducted for 12 h at room temperature under stirring. Following this, a 10 minute centrifugation was performed at 5000 rpm, and the product was collected, cleaned three times with water, and evaporated at 80 °C. Similar to ZIF-8 MOFs, zinc nitrate and CsCl solutions were combined to create ZIF-8 MOFs doped with cesium at different molar ratios of 1 : 10 and 1 : 5 before adding them to the 2-methylimidazole solution. The final products were denoted as Cs-1@ZIF-8 and Cs-2@ZIF-8 MOFs, respectively.

Chemicals

Analytical-grade chemicals were obtained from commercial sources, which were utilized with no additional purification. We purchased 2-methylimidazole, diphenylcarbazide (DCP), and zinc nitrate nonahydrate from Sigma Aldrich (Germany). El Nasr Pharmaceutical Chemicals Co., Egypt, was the supplier of sodium hydroxide, hydrochloric acid, sodium nitrate, sulfuric acid, and acetone.

Adsorption experiments

In a batch mode, sorption investigations were carried out by combining 0.02 g of the Cs-2@ZIF-8 MOF with a solution of 25 millilitres of Cr(VI) (10 mg L⁻¹) and shaking the solutions continuously at 180 rpm. 0.1 mol L⁻¹ HCl and 0.1 mol L⁻¹ NaOH was added to modify the pH of the aqueous solutions. The batch experiments were conducted for five hours at room temperature. Following the filtration process to isolate the adsorbent, the concentration of Cr(VI) ions was measured spectrophotometrically using diphenylcarbazide at 540 nm.[69]

The removal percentage and the quantity of the adsorbed Cr(VI) ions were evaluated using the following equations:

$$\text{removal\%} = \frac{(C_i - C_e)}{C_i} \times 100 \quad (2)$$

$$q_e = (C_i - C_e)V/m \quad (3)$$

where q_e is the amount of adsorbed Cr(VI) (mg g⁻¹) onto the Cs-2@ZIF-8 MOF, C_i, and C_e are the concentrations at the start and end of a given period (mg L⁻¹), m denotes the mass of the Cs-2@ZIF-8 MOF (g), and V stands for the solution volume (L).

Adsorption isotherms

The Cr(VI) adsorption process using the Cs-2@ZIF-8 MOF was investigated using various models, namely the Freundlich, Langmuir, Dubinin–Radushkevich (D–R), and Temkin isotherms. The experimental results were plotted using linear fitting equations, as provided in the SI file, in order to analyze the applicable isotherm models.

Adsorption kinetics

The respective experimental data at various contact times corresponding to changes in the Cr(vi) removal percentage using the Cs-2@ZIF-8 MOF were investigated using different kinetic models (applying nonlinear regression using the equations provided in the SI file Appendix B).

Adsorption thermodynamics

The spontaneity and feasibility of the removal process were assessed using thermodynamic parameters, including Gibbs free energy change (ΔG°), change in entropy (ΔS°), and change in enthalpy (ΔH°), which were computed using the experimental data from adsorption processes employing the following equations:

$$\ln \ K_d = \frac{\Delta S^\circ}{R} - \frac{\Delta H^\circ}{RT} \tag{4}$$

$$\Delta G^\circ = \Delta H^\circ - T\Delta S^\circ \tag{5}$$

where the relation (q_e/C_e) was used to calculate the K_d value. The intercept and slope of the ln K_d *vs.* $1/T$ plots were used to acquire the values of ΔS° and ΔH°. Furthermore, using eqn (5), the Gibbs free energy change (ΔG°) was determined.

Application

The proposed Cs-2@ZIF-8 MOF adsorbent's analytical suitability for removing Cr(vi) from a variety of actual water samples was examined. The samples used were tap water, groundwater, and industrial water.

Conclusions

A Cs-2@ZIF-8 MOF adsorbent was fabricated in this study using a precipitation process and then used to adsorb hexavalent chromium ions in aqueous solutions. To ascertain the materials' composition and structure, XRD, FT-IR, XPS, TEM, SEM, BET, TGA, and PL investigations were used. The findings exhibited that the Cs-2@ZIF-8 MOF had an irregular, dodecahedral structure. The diameters of the crystallites of the Cs-2@ZIF-8 MOF were between 20 and 32 nm, and it got more agglomerated following Cs doping. After the ZIF-8 MOF was doped with Cs ions, its specific surface area increased from 1019.57 to 1204.95 m^2 g^{-1}, according to the results of the BET study employed to characterize the Cs-2@ZIF-8 MOF. It was discovered that at an initial concentration of 10 mg L^{-1} of Cr(vi), the highest capacity for adsorption using the Cs-2@ZIF-8 MOF was 61.05 mg g^{-1}. The study further identified pH 3 as the ideal condition for the removal of Cr(vi) and established strong agreement between the experimental results and both pseudo-second-order kinetic model and the Freundlich isotherm. The process of Cr(vi) removal using the Cs-2@ZIF-8 MOF was spontaneous and exothermic. XRD analysis confirmed that the Cs-2@ZIF-8 MOF preserved its crystalline structure and remained stable even after several adsorption–desorption cycles. In water samples, the high recovery% of Cr(vi) showed how effective the Cs-2@ZIF-8 MOF was at extracting chromium from real samples.

Conflicts of interest

There are no conflicts to declare.

Data availability

All the data generated or analysed during this study are included in this published article and its SI files. The supporting information file contains six figures (Fig. S1–S6), two tables (Table S1 and S2), appendix A for instruments, and appendix B for adsorption isotherms, and adsorption kinetics details. See DOI: **https://doi.org/10.1039/d5va00170f**.

Acknowledgements

Notes and references

1 H. Qi, X. Niu, H. Wu, X. Liu and Y. Chen, *J. Chem.*, 2021, **2021**, 1–9.
2 J. Liu, Y. Ye, X. Sun, B. Liu, G. Li, Z. Liang and Y. Liu, *J. Mater. Chem. A*, 2019, **7**, 16833–16841.
3 M. S. Sreevidya and R. Pavithran, *Mater. Today: Proc.*, 2021, **41**, 479–489.
4 C. Wang, J. Chen and Q. Yang, *Water*, 2023, **16**, 25.
5 B. C. John, V. A. Viswambaram, S. S. Raj and S. A. Mankunipoyil, *Mater. Today Commun.*, 2023, **34**, 105315.
6 R. Acharya, A. Lenka and K. Parida, *J. Mol. Liq.*, 2021, **337**, 116487.
7 G. Hadizade, E. Binaeian and M. R. S. Emami, *J. Mol. Liq.*, 2017, **238**, 499–507.
8 E. Binaeian, H.-A. Tayebi, A. Shokuhi Rad and S. Afrashteh, *J. Macromol. Sci., Part A:Pure Appl. Chem.*, 2018, **55**, 269–279.
9 M. Shabandokht, E. Binaeian and H.-A. Tayebi, *Desalin. Water Treat.*, 2016, **57**, 27638–27650.
10 L. Rani, J. Kaushal, A. L. Srivastav and P. Mahajan, *Environ. Sci. Pollut. Res.*, 2020, **27**, 44771–44796.
11 A. Khosravi, R. Habibpour and M. Ranjbar, *Sci. Rep.*, 2024, **14**, 10736.
12 N. A. A. Qasem, R. H. Mohammed and D. U. Lawal, *npj Clean Water*, 2021, **4**, 36.
13 J. Begum, Z. Hussain and T. Noor, *Mater. Res. Express*, 2020, **7**, 015083.
14 D. Li and F. Xu, *J. Solid State Chem.*, 2021, **302**, 122406.
15 Z. Noraee, A. Jafari, M. Ghaderpoori, B. Kamarehie and A. Ghaderpoury, *J. Environ. Health Sci. Eng.*, 2019, **17**, 701–709.
16 H. Kaur, N. Devi, S. S. Siwal, W. F. Alsanie, M. K. Thakur and V. K. Thakur, *ACS Omega*, 2023, **8**, 9004–9030.
17 M. A. Hamouda, S. M. Sheta, R. R. Sheha, A. T. Kandil, O. I. Ali and S. M. El-Sheikh, *RSC Adv.*, 2022, **12**, 13103–13110.

18 R. R. Sheha, S. M. Sheta, M. A. Hamouda, S. M. El-Sheikh, A. T. Kandil and O. I. Ali, *J. Environ. Radioact.*, 2023, **270**, 107287.

19 S. M. Sheta and S. M. El-Sheikh, *Anal. Biochem.*, 2022, **648**, 114680.

20 X. Zhao, C. Wu, D. Dai, J. Ren, T. Li and S. Ling, *iScience*, 2023, **26**, 107290.

21 Y. Song, Y. Peng, N. V. Long, Z. Huang and Y. Yang, *Appl. Surf. Sci.*, 2021, **542**, 148584.

22 S. A. Ahmed, D. Bagchi, H. A. Katouah, M. N. Hasan, H. M. Altass and S. K. Pal, *Sci. Rep.*, 2019, **9**, 19372.

23 S. M. Sheta, S. M. El-Sheikh, M. M. Abd-Elzaher, M. L. Ghanem and S. R. Salem, *RSC Adv.*, 2019, **9**, 20463–20471.

24 S. M. Sheta, S. M. El-Sheikh and M. M. Abd-Elzaher, *Appl. Organomet. Chem.*, 2019, **33**, e5069.

25 X. Jiang, S. Su, J. Rao, S. Li, T. Lei, H. Bai, S. Wang and X. Yang, *J. Environ. Chem. Eng.*, 2021, **9**, 105959.

26 K. Li, N. Miwornunyuie, L. Chen, H. Jingyu, P. S. Amaniampong, D. Ato Koomson, D. Ewusi-Mensah, W. Xue, G. Li and H. Lu, *Sustainability*, 2021, **13**, 984.

27 J. Huo, L. Xu, J. E. Yang, H. Cui, B. Yuan and M. Fu, *Colloids Surf., A*, 2018, **539**, 59–68.

28 N. Li, L. Zhou, X. Jin, G. Owens and Z. Chen, *J. Hazard. Mater.*, 2019, **366**, 563–572.

29 T. Li, Y. Wang, X. Wang, C. Cheng, K. Zhang, J. Yang, G. Han, Z. Wang, X. Wang and L. Wang, *Membranes*, 2022, **12**, 122.

30 X. Yang, Y. Zhou, Z. Sun, C. Yang and D. Tang, *Colloids Surf., A*, 2020, **603**, 125292.

31 R. Jia, G. Tan, Y. Chen, L. Zuo, B. Li and L. Wang, *Front. Chem.*, 2022, **10**, 1–13.

32 M. Anbia and H. Pazoki, *Appl. Chem. Res.*, 2015, **81**, 73–81.

33 W. Qin, W. Cao, H. Liu, Z. Li and Y. Li, *RSC Adv.*, 2014, **4**, 2414–2420.

34 S. Sun, Z. Yang, J. Cao, Y. Wang and W. Xiong, *J. Solid State Chem.*, 2020, **285**, 121219.

35 B. Shen, B. Wang, L. Zhu and L. Jiang, *Nanomaterials*, 2020, **10**, 1–15.

36 M. Niknam Shahrak, M. Ghahramaninezhad and M. Eydifarash, *Environ. Sci. Pollut. Res.*, 2017, **24**, 9624–9634.

37 R. L. Papurello, L. A. Lozano, E. V. Ramos-Fernández, J. L. Fernández and J. M. Zamaro, *ChemPhysChem*, 2019, **20**, 3201–3209.

38 J. Li, H. Chang, Y. Li, Q. Li, K. Shen, H. Yi and J. Zhang, *RSC Adv.*, 2020, **10**, 3380–3390.

39 H. Mittal, A. Ivaturi and M. Khanuja, *Environ. Sci. Pollut. Res.*, 2023, **30**, 4151–4165.

40 Asha, S. L. Goyal and N. Kishore, *AIP Conf. Proc.*, 2013, **1536**, 617–618.

41 M. Abewaa, A. Arka, T. Haddis, A. Mengistu, T. Takele, E. Adino, Y. Abay, N. Bekele, G. Andualem and H. Girmay, *Results Eng.*, 2024, **22**, 102274.

42 J. Zhang, J. Liu, G. Li, Y. Liu, R. Yang, L. Li, Q. Zhao, J. Gao and H. Lu, *J. Mater. Sci.:Mater. Electron.*, 2023, **34**, 1381.

43 X. Ni, Y. Zhang, C. Xue and X. Chen, *Front. Chem.*, 2022, **10**, 858107.

44 S. Feng, X. Jia, J. Yang, Y. Li, S. Wang and H. Song, *J. Mater. Sci. Mater. Electron.*, 2020, **31**, 22534–22545.

45 S. Chirra, L.-F. Wang, H. Aggarwal, M.-F. Tsai, S. S. Soorian, S. Siliveri, S. Goskula, S. R. Gujjula and V. Narayanan, *Mater. Today Commun.*, 2021, **26**, 101993.

46 L. Zhou, N. Li, G. Owens and Z. Chen, *Chem. Eng. J.*, 2019, **362**, 628–637.

47 J. Ou, Y. Sheu, B. K. Chang, F. Verpoort, R. Y. Surampalli and C. Kao, *Water Environ. Res.*, 2021, **93**, 1995–2009.

48 A. Malik, M. Nath, S. Mohiyuddin and G. Packirisamy, *ACS Omega*, 2018, **3**, 8288–8308.

49 K. Elewa, A. Belal, O. El Monayeri and A. Tawfic, Cu(II) Ion Removal from Aqueous Solution Using Metal-Organic Framework Material, preprints, 2021, vol. 18, pp. 1–10, DOI: **10.20944/preprints202106.0485.v1**.

50 X. Liu, H. Liu, K. Cui, Z. Dai, B. Wang, R. Weerasooriya and X. Chen, *Water*, 2023, **15**, 2290.

51 S. Sulaiman, R. S. Azis, I. Ismail, H. C. Man, K. F. M. Yusof, M. U. Abba and K. K. Katibi, *Nanoscale Res. Lett.*, 2021, **16**, 168.

52 T. Chowdhury, L. Zhang, J. Zhang and S. Aggarwal, *Mater. Adv.*, 2021, **2**, 3051–3059.

53 X. Lv, Y. Hu, J. Tang, T. Sheng, G. Jiang and X. Xu, *Chem. Eng. J.*, 2013, **218**, 55–64.

54 A. M. Saleh, H. H. Mahdi, A. B. Alias, N. K. A. Hadi, D. Qarizada, A. H. Jawad and N. M. Saleh, *Desalin. Water Treat.*, 2024, **317**, 100149.

55 H. Fei, C. S. Han, J. C. Robins and S. R. J. Oliver, *Chem. Mater.*, 2013, **25**, 647–652.

56 H. Fei, M. R. Bresler and S. R. J. Oliver, *J. Am. Chem. Soc.*, 2011, **133**, 11110–11113.

57 P. F. Shi, B. Zhao, G. Xiong, Y. L. Hou and P. Cheng, *Chem. Commun.*, 2012, **48**, 8231–8233.

58 L. L. Li, X. Q. Feng, R. P. Han, S. Q. Zang and G. Yang, *J. Hazard. Mater.*, 2017, **321**, 622–628.

59 X. Li, X. Gao, L. Ai and J. Jiang, *Chem. Eng. J.*, 2015, **274**, 238–246.

60 J. Wen and X. Hu, *J. Colloid Interface Sci.*, 2021, **589**, 578–586.

61 N. S. Alsaiari, M. S. Alsaiari, F. M. Alzahrani, A. Amari and M. A. Tahoon, *Rev. Adv. Mater. Sci.*, 2023, **62**, 20230145.

62 C. E. Almeida-naranjo, M. Belén, G. Cabrera and V. H. Guerrero, *Environ. Challenges*, 2021, **5**, 100343.

63 N. F. Al-Harby, E. F. Albahly and N. A. Mohamed, *Polymers*, 2021, **13**, 4446.

64 K. Zhu, C. Chen, H. Xu, Y. Gao, X. Tan, A. Alsaedi and T. Hayat, *ACS Sustain. Chem. Eng.*, 2017, **5**, 6795–6802.

65 X. Hu, J. Wen, H. Zhang, Q. Wang, C. Yan and L. Xing, *Chem. Eng. J.*, 2020, **391**, 123501.

66 K. D. Nguyen, P. H. Ho, P. D. Vu, T. L. D. Pham, P. Trens, F. Di Renzo, N. T. S. Phan and H. V Le, *Nanomaterials*, 2021, **11**, 1398.

67 M. D. Yahya, A. S. Aliyu, K. S. Obayomi, A. G. Olugbenga and U. B. Abdullahi, *Cogent Eng.*, 2020, **7**, 1748470.

68 T. S. Badessa, E. Wakuma and A. M. Yimer, *BMC Chem.*, 2020, **14**, 71.

69 S. M. El-Sheikh, A. B. Azzam, R. A. Geioushy, F. M. El Dars and B. A. Salah, *J. Alloys Compd.*, 2021, **857**, 157513.